



Optimization Optoelectronic Properties $\text{Zn}_x\text{Cd}_{1-x}\text{Te}$ System for Solar Cell Application: Theoretical and Experimental Study

Nematov Dilshod Davlatshoevich ^{1,2,*} , Makhsudov Barot Islomovich ³, Kholmurodov Kholmirzo Tagoykulovich ^{4,5} , Yarov Muhammadjon Temurjonovich ³

¹ S.U.Umarov Physical-Technical Institute of National Academy of Sciences of Tajikistan

² M.S.Osimi Tajik Technical University, Dushanbe, 724000 Tajikistan

³ Tajik National University, Tajikistan

⁴ Joint Institute for Nuclear Research, Dubna, Moscow Region, 141980 Russia

⁵ Dubna State University, Dubna, Moscow Region, 141980 Russia

* Correspondence: dilnem@mail.ru (N.D.D.);

Scopus Author ID 57210187257

Received: 8.12.2021; Accepted: 5.01.2022; Published: 12.02.2022

Abstract: Within the framework of the density functional theory (DFT) using the Wien2k package and the method of linear extended plane waves (FP-LAPW), quantum mechanical calculations were implemented to study the structural, electronic, and optical properties of the $\text{Zn}_x\text{Cd}_{1-x}\text{Te}$ system in the full range of $0 \leq x \leq 1$ with a step of 0.25. To determine the optimal volume and grid parameters, the calculation of the total energy of semiconductor nanocomposites CdTe, $\text{Zn}_{0.25}\text{Cd}_{0.75}\text{Te}$, $\text{Zn}_{0.5}\text{Cd}_{0.5}\text{Te}$, $\text{Zn}_{0.75}\text{Cd}_{0.25}\text{Te}$, and ZnTe, the generalized gradient approximation (GGA) was applied, which is based on relaxation (optimization) of the volume and minimization of energy (finding the energy of the ground state). According to our calculations within the framework of the DFT, with an increase in the Zn concentration, the constant lattice parameters and the size (volume) of these nanocrystals decrease and are in good agreement with the results obtained this work by the method of X-ray structural analysis. The calculated band gaps of these nanocrystals using the modified exchange-correlation potential mBJ tend to increase, which agrees with the experimental data. The results of spin-polarized and spin-orbit calculations of the band structure showed that all these nanocrystals have direct transition points for electrons. After approximation by the least-squares method, empirical formulas were obtained to establish the concentration dependence of changes in the volumes and bandgap of Zn-modified nanocrystals, which will help experimenters obtain particles with certain sizes and bandgap. Such theoretical studies further open the possibility of accurate prediction of the electronic-energy properties of other semiconductor nanosized structures to develop and produce new nanomaterials with predetermined and programmed properties.

Keywords: cadmium telluride; doping; density functional calculation; X-ray analyses; electronic properties; band gap; optical properties; absorption coefficient; dielectric constant.

© 2022 by the authors. This article is an open-access article distributed under the terms and conditions of the Creative Commons Attribution (CC BY) license (<https://creativecommons.org/licenses/by/4.0/>).

1. Introduction

With rapidly increasing emissions of greenhouse gases into the atmosphere, it is important to develop technologies that can generate energy at a low cost to the environment and reverse the currently intensifying climate change. However, to successfully make the transition from fossil fuels to renewable energy sources, humanity cannot rely solely on

existing materials but must focus on the synthesis of other classes of substances, especially nanomaterials with improved and easily controllable properties. Conventional energy production methods will not be able to meet the energy needs of the 'world's population. Therefore, unconventional measures like creating photovoltaic devices and wind farms are of great interest [1-3]. Type II-VI semiconductor materials have found their application in many branches of science and technology, such as photovoltaic and photoconductive devices [4].

On the other hand, heteronanojunctions (HNJs) have attracted intense research interest over the past four decades [5] because of their potential importance in many technological problems. Cadmium telluride (CdTe) is unique among II-VI compounds, making it important and highly suitable for several such applications since it can exhibit both n- and p-type conductivity. It is one of the few compounds II-VI that is commonly used as an absorber for photovoltaic devices [6-9]. In addition, CdTe can be easily doped with p- and n-type semiconductors. Elements of the first and fifth columns of the periodic table act as acceptors, and elements of the third and seventh columns act as donors. Some of these elements exhibit special behavior in CdTe, depending on their place (position) in the crystal lattice. In recent years, work intensively obtained high-class CdZnTe crystals at a low cost. Due to their working potential at room temperature, nanosized CdZnTe alloys are very important for nuclear detectors [10,11]. Moreover, it is reported that the possibility of using nanosized alloys $\text{Zn}_{1-x}\text{Cd}_x\text{Te}$ to develop X-ray detectors of gamma radiation and the manufacture of optoelectronic devices and solar cells that operate in the blue-green region of the spectrum [12,13]. On the other hand, CdTe nanoscale thin-film technology has a prominent place in the solar energy market and, therefore, may offer a natural alternative. Another advantage of thin films is that they can be synthesized by several available physicochemical methods, such as chemical bath deposition, spray pyrolysis, thermal evaporation, electrodeposition, sputtering, and pulsed laser ablation (ILD). Moreover, nanosized crystals based on CdTe have a high optical absorption coefficient of about 10^4 cm^{-1} and absorb about 92% of visible light. This efficiency is much higher than crystalline silicon, based on which tandem solar panels have been prepared recently. Therefore, it is possible to use CdTe nanocrystals and thin films to produce efficient solar cells with reduced recombination losses and improved current density.

The bandgap is 1.5 eV for pure CdTe, just in the middle of the solar spectrum, and has a high absorption coefficient for the visible solar spectrum [14]; however, to obtain maximum performance, the bandgap of CdTe must be increased to 1.8 eV [15,16], because according to the Shockley-Keisser limit [17], the maximum conversion efficiency is achieved for materials with a bandgap of 1.5 eV and more [18], and also the spectrum of solar radiation received by the Earth has a maximum intensity at a wavelength almost corresponding to photons with an energy of 1.5 eV [18]. However, it is known that for mixed semiconductor materials such as CdTe and its alloys, the maximum efficiency (Shockley-Keisser limit) is achieved for shorter wavelengths. Therefore, it is necessary to increase the bandgap and optimize the absorption capacity of CdTe for beams with energies above 1.5 eV. This can be achieved by doping foreign ions such as Zn or Mg in the CdTe supercell. One of the advantages of this material is the ability to control and regulate the bandgap with different impurity concentrations. Doping with Zn causes a significant change in CdTe thin films' optical, electrical, and mechanical properties. Nanocrystals of the $\text{Zn}_{1-x}\text{Cd}_x\text{Te}$ system with a low Zn content (up to 20%), in particular, have been carefully studied for radiation detectors (gamma and X-ray radiation) [19], which showed a higher electrical resistance and lower density defects compared to pure CdTe. However, low concentrations have been shown to introduce little change in bandgap optimization.

Considering the above points, the purpose of this work is to study the effect of the percentage of Zn doping on the structural (dimensional) and electronic properties of the $\text{Zn}_{1-x}\text{Cd}_x\text{Te}$ system in the full range of $0 \leq x \leq 1$ with all possible doping concentrations. Doping is carried out by replacing Cd atoms with Zn in the CdTe cell.

2. Materials and Methods

2.1. Experimental section.

The experimental part of the work consists of X-ray structural analysis of pure CdTe crystals, which were obtained in [20-25] for use in nuclear detectors with high radiation resistance by vacuum deposition. X-ray structural analysis of CdTe crystals was performed on a DRON-3.0 diffractometer. The samples were examined at angles from 10° to 60° along 2θ . The X-ray source was operated with an emission current of 6 mA, and the voltage between the cathode and anode in the X-ray tube was 36 kV. Ordinary water was used to cool the anode. Since single crystals were used in X-ray diffraction analysis, the maximum direction of X-ray diffraction is determined following the Wolf-Bragg condition:

$$2d \sin \theta = n\lambda \quad (1)$$

Experimental analysis can confirm that theoretical calculations based on DFT can give correct estimates of the lattice parameters, completely independent of the experiment.

2.2. Theoretical part.

To study the structural and electronic properties of the $\text{Zn}_{1-x}\text{Cd}_x\text{Te}$ system, quantum-mechanical calculations were implemented using the density functional theory (DFT), as well as the extended plane wave (FP-LAPW) code, the Wien2k package with the generalized gradient approximation GGA-PBE (for geometry optimization), and a modified exchange-correlation potential mBJ (for calculating electronic properties).

The initial data for calculations were the parameters of the CdTe cubic phase with the space group (F-43m) and number 406 in the Material Projects crystallographic database [26] with fixed atomic positions for Cd, Te, and Zn. The radius of the Muffin sphere (ion radius) for Cd, Te, and Zn was taken as $2.5a_0$, where a_0 is the Bohr radius. After doping with a certain concentration of zinc, optimization steps were implemented for all nanocrystals of the $\text{Zn}_{1-x}\text{Cd}_x\text{Te}$ system. In fig. 1 (a - e) shows the optimized crystal structures $2 \times 2 \times 2$ - supercells CdTe, $\text{Zn}_{0.25}\text{Cd}_{0.75}\text{Te}$, $\text{Zn}_{0.5}\text{Cd}_{0.5}\text{Te}$, $\text{Zn}_{0.75}\text{Cd}_{0.25}\text{Te}$, and ZnTe. The three-dimensional structures of the crystal lattice of these systems were visualized by the VESTA.

The total energy minimization is performed using convergence steps that include lattice relaxation, energy convergence, and k-convergence to obtain a stable ground state structure. The optimization of crystal structures was carried out by the Murnaghan method, which, in connection with *ab initio* calculations, would be preferable to express the energy as a function of volume:

$$E(V) = E_0 + BV_0 \left[\frac{1}{B'(B'-1)} \left(\frac{V_0}{V} \right)^{1-B'} + \frac{V}{B'V_0} - \frac{1}{B'-1} \right] \quad (2)$$

where B - bulk modulus, B' - pressure derivative of the volumetric modulus ($B' = (\partial B / \partial P)_T$), V_0 - equilibrium volume, that is, when the system is in a relaxing (ground) state.

To determine the bandgap, it is necessary to calculate the total energy. The minimization and calculation of the total energy of a many-electron system are performed

according to the Kohn - Sham rules [27], based on two Hohenberg - Kohn theorems [28], and begins with writing the Schrödinger equation in the form:

$$\left(\frac{\hbar^2}{2m} \nabla^2 + E_{ion}(r) + E_h(r) + E_{xc}(r) \right) \psi_i(r) = E \psi_i(r) \quad (3)$$

Here $E_{ion}(r)$ is the ionic potential, $E_h(r)$ - Hartree potential, and $E_{xc}(r)$ is the exchange-correlation potential. The last 2 potentials are calculated as:

$$E_h(r) = e^2 \int \frac{\rho(r')}{|r-r'|} dr' \quad (4)$$

$$E_{xc}(r) = \frac{\delta \epsilon_{xc}[\rho(r)]}{\delta \rho(r)} \quad (5)$$

where $\rho(r)$ is the electron density functional.

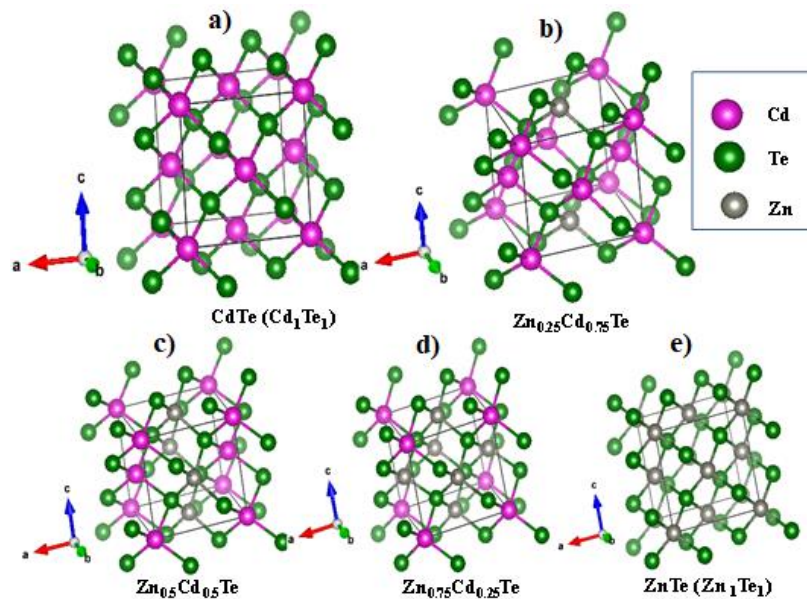


Figure 1 (a, e). Crisallic structures (a) CdTe, (b) $\text{Zn}_{0.25}\text{Cd}_{0.75}\text{Te}$, (c) $\text{Zn}_{0.5}\text{Cd}_{0.5}\text{Te}$, (d) $\text{Zn}_{0.75}\text{Cd}_{0.25}\text{Te}$ and (e) ZnTe.

Hohenberg and Kohn showed in 1964 within the framework of the DFT that the electron density functional $\rho(r)$ for the normalized ψ is defined as

$$\rho(r) = N \int d^3r_2 \dots \int d^3r_N \psi^*(\vec{r}, \vec{r}_2, \dots, \vec{r}_N) \psi(\vec{r}, \vec{r}_2, \dots, \vec{r}_N) \quad (6)$$

For the density of the ground state $\rho_0(r)$, it is possible in principle to calculate the corresponding wave function of the ground state $\psi_0(r_1, \dots, r_N)$, where N is the number of electrons. In other words, ψ is a unique functional of $\rho_0(r)$.

$$\psi_0 = \psi(\rho_0) \quad (7)$$

Thus, the density functional is defined as:

$$\rho(r) = \sum_{\text{states } i} \psi_i^*(r) \psi_i(r) \quad (8)$$

In the framework of Wien2k, the corresponding $\rho(r)$, E_h and E_{xc} are first calculated, and then the solution of the Schrödinger equation (equation 3) is carried out. Then, from the eigenstates ($\psi_i(r)$), the $\rho(r)$ is calculated using Eq. 8.

The energy of the bandgap within the modified Becke and Johnson potential [29] is determined by the following equation:

$$E_{xc}^{mBJ}(r) = cE_x^{BR}(r) + (3c - 2) \frac{1}{\pi} \sqrt{\frac{5k(r)}{6\rho(r)}} \quad (9),$$

where $k(r)$ is the kinetic energy density according to the Kohn - Sham equation, is the spin-dependent electron density, and E_x^{BR} - is the Becke - Roussel exchange functional (BR) [30]. The parameter c was proposed to be determined self-consistently depending on the electron density, as:

$$c = \alpha + \beta g^p, \quad (10)$$

where

$$g = \frac{1}{V_{cell}} \int \frac{|\nabla \rho(r')|}{\rho(r')} d^3 r' \quad (11)$$

The constants of equation 6 were taken as $\alpha = -0.012$, $\beta = 1.023 B^{1/2}$, and $p = 1/2$ after minimizing the average absolute error of the bandgap for a wide range of solids [31].

The optical properties of the $Zn_{1-x}Cd_xTe$ system were investigated using their real (ϵ_1) and imaginary (ϵ_2) parts of the permittivity [32-43], and then the optical conductivity (σ), as well as the extinction (k) and absorption (α) coefficients as:

$$k = \sqrt{\epsilon_2} \quad (12)$$

$$\alpha = \frac{4\pi}{\lambda} k \quad (13)$$

$$\sigma = \frac{1}{2} \frac{c}{\lambda} \epsilon_2 \quad (14),$$

For all our calculations of the convergence criterion, the total energy was taken to be 10^{-5} eV, and the forces per atom were reduced to 10^{-3} eV. The valence wave functions inside the MT sphere were expanded to $l_{max} = 10$ (the maximum order of the spherical harmonic used in the expansion), and the charge density was expanded in a Fourier series up to G_{max} (Bohr⁻¹) (the summation boundary over reciprocal lattice vectors). The calculations were carried out in the irreducible Brillouin zone according to the Monkhorst-Pack scheme [44] and a $2 \times 2 \times 2$ k-point grid. The kinetic cutoff energy of a plane wave is set at 400 eV for all calculations.

3. Results and Discussion

3.1. Structural properties.

The calculated optimized structural parameters for all nanocrystals of the $Zn_xCd_{1-x}Te$ system are given in Table 1. The calculation results are in table 1, and figure 2 show a linear decrease in the lattice constant and volumes of these systems with increasing zinc concentration, which ideally obey 'Vegard's law.

Table 1. The meaning of structural parameters $Zn_xCd_{1-x}Te$.

$Zn_xCd_{1-x}Te$	Lattice parameters and system volume			Error in a, %
	This work		Experiment	
	$a=b=c, \text{\AA}$	$V, \text{\AA}^3$	$a=b=c, \text{\AA}$	
CdTe	6.7364	305.7004	6.5 [45]	3.5
$Zn_{0.25}Cd_{0.75}Te$	6.6299	291.4278	-	-
$Zn_{0.5}Cd_{0.5}Te$	6.5140	280.1688	-	-
$Zn_{0.75}Cd_{0.25}Te$	6.4496	268.2909	-	-
ZnTe	6.3774	259.3805	6.103 [46], 6.20 [47]	4.37, 2.7

Least squares corresponding to the calculated volume of these nanoparticles, shown by the solid line in Fig. 2, are expressed by the formula $V = -11.578x + 315.73$, from which it is possible to estimate the volume of these nanocrystals of the $Zn_xCd_{1-x}Te$ system for any other concentration of Zn, in the range $0 < x < 1$.

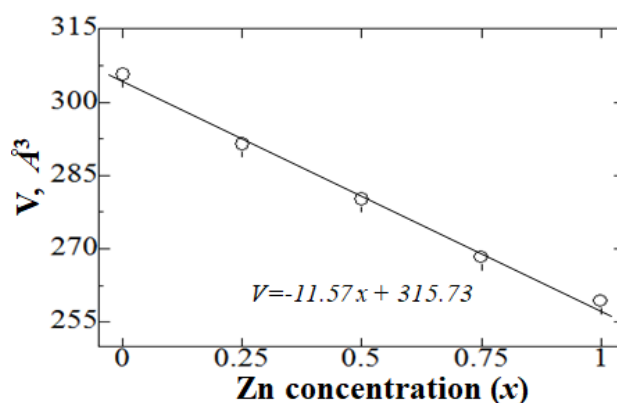


Figure 2. The dependence of the volume on the Zn content for $\text{Zn}_x\text{Cd}_{1-x}\text{Te}$ samples.

Figure 3 (a) compares the obtained X-ray diffraction patterns from the experiment (DRON 3) and powder X-ray patterns obtained from the optimized geometry using the REFLEX software included in the Materials Studio software package with CuK α radiation ($\lambda = 1.54 \text{ \AA}$).

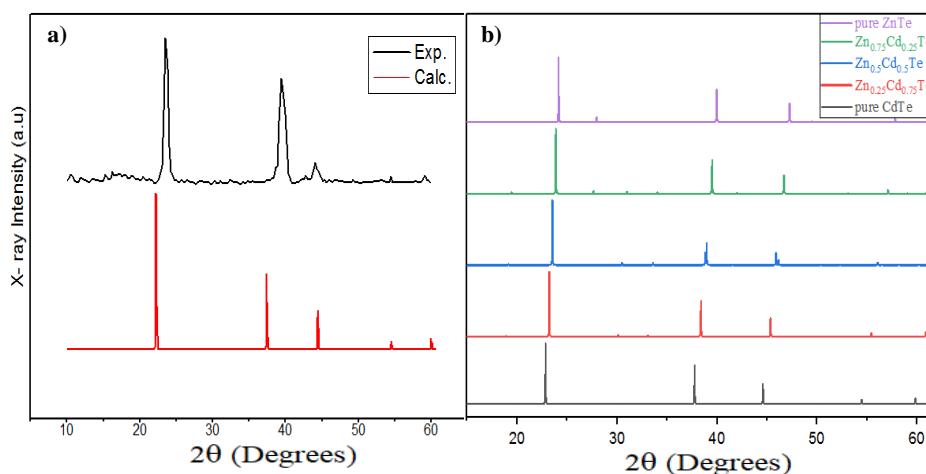


Figure 3 (a, b). Calculated and experimental X-ray diffraction patterns for pure CdTe (a) and powder diffraction patterns (b) for the $\text{Zn}_x\text{Cd}_{1-x}\text{Te}$ system.

According to the results of our quantum-chemical calculations (Fig. 3 (b)), for the $\text{Zn}_x\text{Cd}_{1-x}\text{Te}$ system, one can notice a change in the interplanar spacing since, with an increase in the Zn concentration, displacements and shifts of the peaks are observed diffractograms towards large angles. The data obtained from first-principle calculations in the form of unit cell parameters, bond lengths, and angles, as well as a powder X-ray diffraction pattern, have excellent agreement with their experimental counterparts from this work and other experiments; therefore, the DFT method is used to carry out the remaining theoretical calculations on the electron-energy and spectral properties displaced cadmium telluride crystals.

3.2. Electronic properties.

The electronic properties of the $\text{Zn}_x\text{Cd}_{1-x}\text{Te}$ system were estimated in the form of the bandgap, the distribution of energy bands, and the dependence of the energy of the bandgap (Bandgap) on the density of electronic states (DOS) in the unit cell, since understanding their formation is considered vital for the development and manufacture of photovoltaic devices based on CdTe and other materials. Table 2 compares the band gap values we calculated within

the DFT, and I fixed and added this link above exchange-correlation potentials LDA, GGA, and mBJ (TB-mBJ) with experimental data.

Table 2. Bandgap values calculated with LDA, GGA, and mBJ for $\text{Zn}_x\text{Cd}_{1-x}\text{Te}$ system in comparison with experimental results.

System		CdTe	$\text{Zn}_{0.25}\text{Cd}_{0.75}\text{Te}$	$\text{Zn}_{0.5}\text{Cd}_{0.5}\text{Te}$	$\text{Zn}_{0.75}\text{Cd}_{0.25}\text{Te}$	ZnTe
Band gap, eV	This work	LDA	0.800	0.996	1.186	1.332
		GGA	0.758	0.839	1.023	1.270
		mBJ	1.501	1.672	1.788	2.169
	Experiment	1.5 [48,49]	-	-	-	2.25 [49]

Figure 4 shows the dependence of the change in the bandgap value on the change in the zinc content in the system. The bandgap value increases according to the law $E_{Bg} = 0.6016x + 1.4932$, where x is the concentration of zinc in the range $0 < x < 1$. Typically, these least-squares allow us to find the bandgap value for the remaining intermediate zinc concentrations.

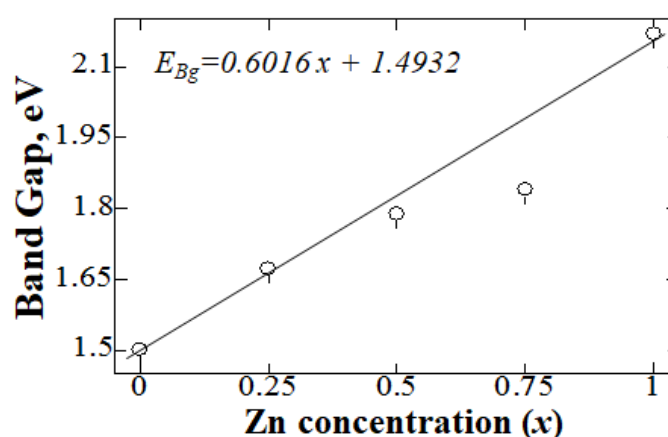


Figure 4. The dependence of the BandGap energy on the Zn content for $\text{Zn}_x\text{Cd}_{1-x}\text{Te}$ samples.

The results of our calculations for estimating the bandgap of pure tellurides (CdTe and ZnTe) agree with the experiment with high accuracy, which confirms the correct choice of the exchange-correlation functional for these systems, as well as the correctness and reliability of calculations within the DFT framework. It can be seen that the bandgap increases linearly. Still, the linearity is violated for some doping concentrations, and the bandgap deviates from the true value, which may be due to the quantum nature of these systems or to errors in our quantum chemical calculations.

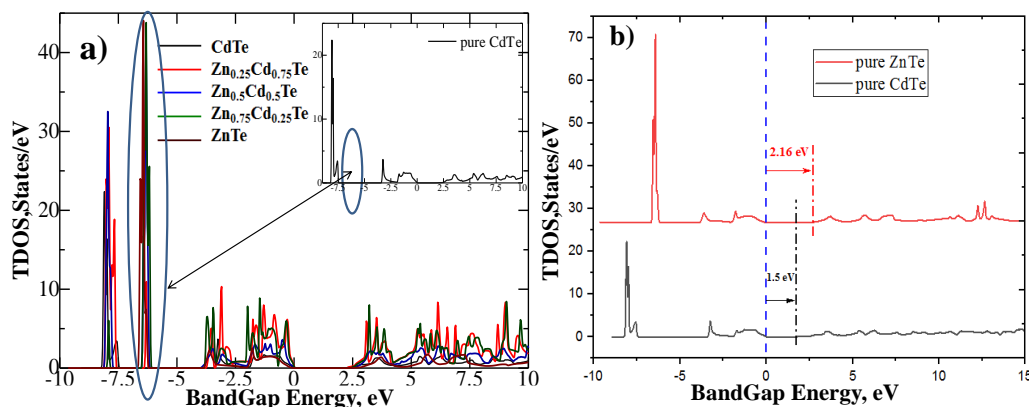


Figure 5(a, b). The total density of states for the $\text{Zn}_x\text{Cd}_{1-x}\text{Te}$ system (a) and comparison of the density of electronic states of pure CdTe and ZnTe (b).

The calculated total density of electronic states of the structurally optimized $\text{Zn}_x\text{Cd}_{1-x}\text{Te}$ models described above is shown in Fig. 5 (a). The Fermi level is marked with dashed lines, which are located at point zero.

The calculated density of states (DOS) of these materials is discussed in terms of the contribution of the constituent atoms' various s-, p-, and d-states. The graphs of the charge density distribution are analyzed. It can be seen that with increasing concentration, the bandgap and the density of electronic states increase (Fig. 5 (a, b)), and new energy levels appear in the negative energy region due to p-electrons of Zn orbitals, which are absent in the band diagram of pure cadmium telluride (Fig. 5 (a)). The densities of electronic states for terminal elements (CdTe and ZnTe) in Figure 5 (b) suggest that pure tellurides are characterized by low densities of states in the conduction band compared to their shifted compositions. However, with an increase in the zinc concentration in the $\text{Zn}_x\text{Cd}_{1-x}\text{Te}$ system and the transition to the ZnTe system, the density of states is observed in both bands.

It can be seen that with increasing concentration, the bandgap and the density of electronic states increase, and new energy levels appear in the negative energy region due to p-electrons of Zn orbitals, which are absent in the band diagram of pure cadmium telluride (Fig. 6 (a-e)).

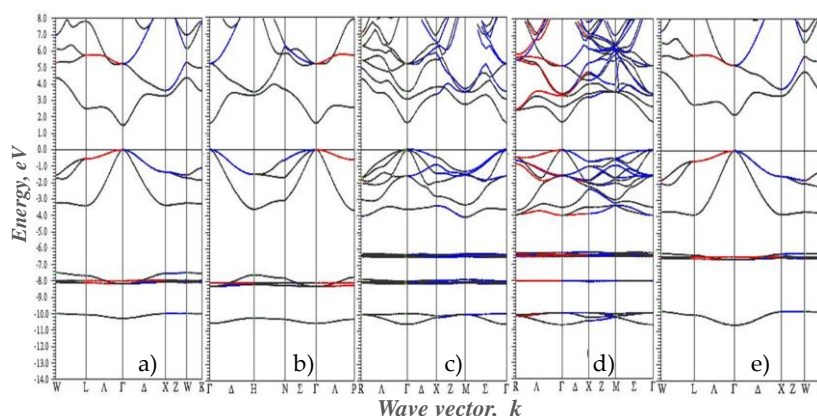


Figure 6 (a-e). Calculated bandstructure (energy diagram) for: (a) CdTe, (b) $\text{Zn}_{0.25}\text{Cd}_{0.75}\text{Te}$, (c) $\text{Zn}_{0.5}\text{Cd}_{0.5}\text{Te}$, (d) $\text{Zn}_{0.75}\text{Cd}_{0.25}\text{Te}$, and (e) ZnTe. The position of the Fermi level is at 0 eV.

The energy band diagram in Figure 4 indicates that all of these materials have a direct transition band structure, which means they are quite suitable for use as optical materials of interest. The calculated band structures show a direct bandgap for all three alloys with an increasing order in the entire range of values of the composition parameter x (Zn concentration).

3.3. Optical properties.

The optical parameters of materials, such as the imaginary (ϵ_2) part of the dielectric constant, absorption coefficient, an extinction coefficient, indicate what type of response these materials will exhibit when photons are incident on them. Based on this, the optical properties of the $\text{Zn}_x\text{Cd}_{1-x}\text{Te}$ system are explained using their real (ϵ_1) and imaginary (ϵ_2) parts of the dielectric functions. The real part indicates the accumulated energy of the material, which can be delivered at zero energy or at the zero frequency limit, which is considered an intrinsic characteristic of any material. On the other hand, the imaginary part (ϵ_2) represents the absorption capacity; however, basically, it gives us information about how the material reacts

when the disturbance is caused by electromagnetic radiation and directly depends on its band structure.

Figure 7 (a, b) shows the graphs of the dependence of ϵ_1 and ϵ_2 on the energy of incident photons for all nanocrystals of the $\text{Zn}_x\text{Cd}_{1-x}\text{Te}$ system ($0 \leq x \leq 1$).

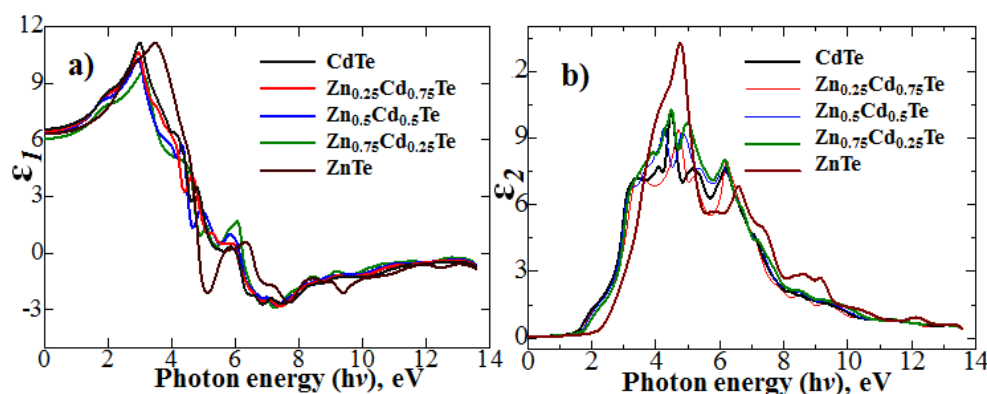


Figure 7 (a, b). Calculated real (a) and imaginary (b) parts of the dielectric constant of $\text{Zn}_x\text{Cd}_{1-x}\text{Te}$ system.

Typically, when light propagates in an elastic medium, light dissipation occurs, the cause of which is the scattering and absorption of light. This phenomenon is called extinction. In other words, extinction means how actively rays with a certain wavelength are absorbed in a material. The extinction coefficient (k) measures the extinction of light. Figure 8 shows the dependences of the extinction coefficients of the investigated materials on the photon energy.

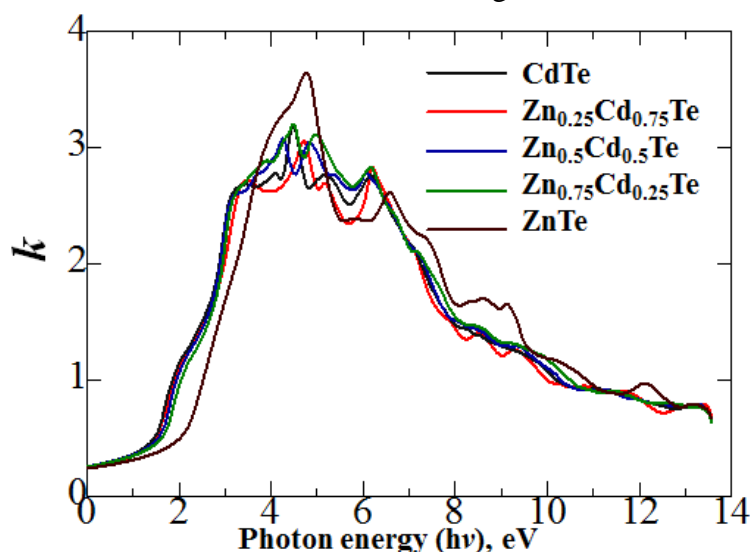


Figure 8. The dependence of the extinction coefficient on the photon energy for the $\text{Zn}_x\text{Cd}_{1-x}\text{Te}$ system.

A negative value for ϵ_1 indicates their metallic nature. That is, at a sufficiently high value of the incident photon energy, the $\text{Zn}_x\text{Cd}_{1-x}\text{Te}$ systems exhibit metallic behavior. It is possible to investigate and evaluate the metallicity of a compound by a real function.

At low scattering and high absorptions, the extinction coefficient becomes the same as the absorption coefficient. Figures 9 (a, b) show the absorption capacity and optical conductivity of the systems understudy for the infrared and visible range of solar radiation since materials active in infrared and visible radiation are generally suitable for tendemic photovoltaic devices.

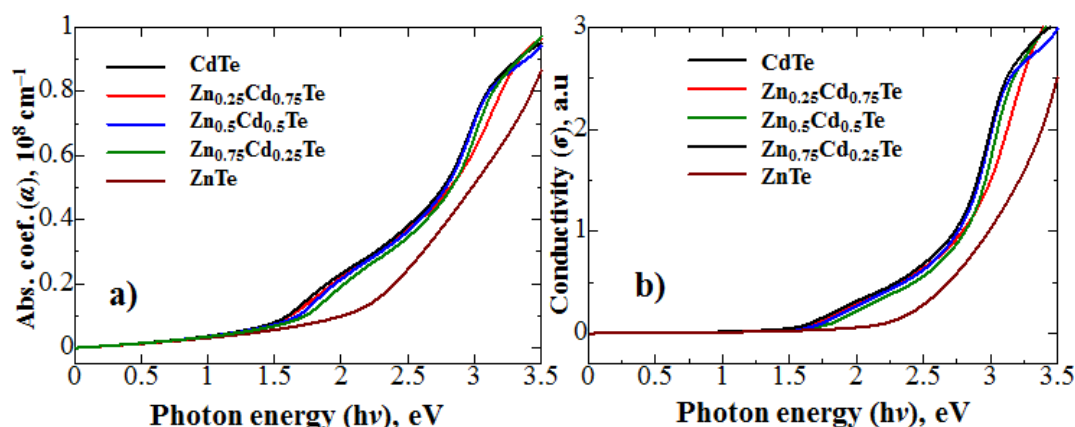


Figure 9(a, b). Calculated absorption coefficient (a) and optical conductivity (b) function of photon energy for the $\text{Zn}_x\text{Cd}_{1-x}\text{Te}$ system.

The absorption coefficient (α) determines the depth of penetration of light to its total absorption. This process depends on the wavelength (energy) of the photon and the intrinsic properties of the material [50,51]. The calculated maxima of extinction (Fig. 8) and absorption (Fig. 9 (a)) are in the same energy range, which is confirmed with the theory of dispersion [52-55]. The optical conductivity spectra $\sigma(\omega)$ calculated in the low-energy range in Fig. 9 (a) show several peaks corresponding to bulk plasmon emissions caused by electrons passing from the valence band to the conduction band. $\sigma(\omega)$ values in the low energy range correspond to interband and intraband transitions, respectively.

The results obtained are in very good agreement with the results of other authors [56-59] and may contribute to the understanding of some features of the optical properties that are important for the practical application of the systems under study and may be of interest to researchers looking for materials with predetermined and programmed optoelectronic characteristics.

4. Conclusions

Zinc doping of the CdTe crystal lattice increased the bandgap to an optimal value, which led to the fact that $\text{Zn}_x\text{Cd}_{1-x}\text{Te}$ nanoparticles can become a promising candidate for work in thin-film solar cells as an absorber layer. The obtained results of studies of the electronic properties of these materials were compared with existing experimental data and other theoretical calculations. It was found that new energy levels appear for displaced tellurides in the region of negative energies due to the p-electrons of the Zn orbitals, absent in the band diagram of pure cadmium telluride and zinc telluride. The absorption spectra of the studied nanocrystals show that with an increase in the Zn concentration, the absorption edges shift towards shorter waves. At the same time, it became known that the optimal concentration of Zn ($x = 0.75$) effectively increases α . The results obtained can be used by other researchers to model the structure of CdTe - similar systems that are supposed to be synthesized and determine such important characteristics as “composition-structure-property”.

Funding

The research leading to these results has received funding from the European Union’s Horizon 2020 research and innovation program under the Marie SkłodowskaCurie grant agreement 871284 project SSHARE.

Acknowledgments

The authors express their deep gratitude and gratitude to the Professor of the Laboratory of Materials Science, Waseda University, respected Tamoyuki Yamamoto for valuable advice and presentation of computing clusters with software Wien2k.

Conflicts of Interest

The authors declare no conflict of interest.

References

1. Timperley, J.; V. Why fossil fuel subsidies are so hard to kill.. *Nature* **2021** 598 (7881),403-405, doi: 10.1038/d41586-021-02847-2.
2. Al-Maamary, H.M.; Kazem, H.A.; Chaichan, M.T. Climate Change: The Game Changer in the GCC Region. *Renewable and Sustainable Energy Reviews* **2017**, 76, 555-576, <https://doi.org/10.1016/j.rser.2017.03.048>.
3. Roshen, T.A.; Sanaa, A.H.; Hussein, A.K.; Miqdam, T.C. Humidity impact on photovoltaic cells performance: A review. *Techno-Economical Assessment of Photovoltaic Systems* **2018**, 3, 27-37.
4. Yanhong, L.; Fenghua, L.; Hui, H.; Baodong, M.; Yang, L.; Zhenhui, K. Optoelectronic and photocatalytic properties of I–III–VI QDs: Bridging between traditional and emerging new QDs. *Journal of Semiconductors* **2020**, 41, <https://doi.org/10.1088/1674-4926/41/9/091701>.
5. Yu, F. Structure of CdTe /Cd_{0.959} Zn_{0.041}Te, Hg_{1-x}C_xTe, CdTe, CdTe . GaAs Heterojunctions. *Journal of Crystal Growth* **1999**, 205, 264-269, [https://doi.org/10.1016/S0022-0248\(99\)00276-6](https://doi.org/10.1016/S0022-0248(99)00276-6).
6. Morales, A. Thin Film CdS. CdTe Solar Cells: Research Prospects. *Solar Energy* **2006**, 80, 675-681, <https://doi.org/10.1016/j.solener.2005.10.008>.
7. Bhanu, M.; Venkata, S.; Sriram, M.; Hussien, M.; Syam, S.; Basavaiah, C. Photocatalytic Activity of Heavy Metal Doped CdS Nanoparticles Synthesized by Using Ocimum sanctum Leaf Extract. *Biointerface Research in Applied Chemistry* **2021**, 11, 12547-12559, <https://doi.org/10.33263/BRIAC115.1254712559>.
8. Masafumi, Yamaguchi. Multi-junction solar cells paving the way for super high-efficiency. *Journal of Applied Physics* **2021**, 129, 240901 (2021); <https://doi.org/10.1063/5.0048653>
9. Najm, A.S.; Moria, H.; Ludin, N.A. Areca catechu as photovoltaic sensitizer for dye-sensitized solar cell (DSSC). *Biointerface Research in Applied Chemistry* **2020**, 10, 5636-5639, <https://doi.org/10.33263/briac103.636639>.
10. Schieber, M.; Schlesinger, T.; James, R.; Hermon, H.; Yoon, H.; Goorsky, M. Point Defects in CdZnTe Crystals Grown by Different Techniques. *J. Crystal Growth* **2002**, 3, 237-239, <https://doi.org/10.1007/s11664-010-1504-x>.
11. Roy, U.N.; Camarda, G.S.; Cui, Y.; James, R.B. Advances in CdZnTeSe for Radiation Detector Applications *Radiation* **2021**, 1, 123–130, <https://doi.org/10.3390/radiation1020011>.
12. Alam, M.D.; Nasim, S.S.; Hasan, S. Recent progress in CdZnTe based room temperature detectors for nuclear radiation monitoring. *Progress in Nuclear Energy* **2021**, 140, <https://doi.org/10.1016/j.pnucene.2021.103918>.
13. Pavlyuk, M.D.; Kanevsky, V.M.; Dvoryankin, V.F.; Kudryashov, A.A.; Petrov, A.G.; Ivanov, Y.M. Detectors for Digital X-Ray Imagers Manufactured of Melt-Grown CdTe and CdZnTe Single Crystals. *Nucl. Instrum. Methods Phys. Res. A* **2010**, 624, 482–485, <https://doi.org/10.1016/j.nima.2010.03.158>.
14. Lane, D. Review of the Optical Band gap of Thin Film. CdS_xTe_{1-x}. *Solar Power Materials and Solar Cells* **2006**, 90, 1169-1175, <https://doi.org/10.1016/j.solmat.2005.07.003>.
15. Koç, M.; Kartopu, G.; Yerci, S. Combined Optical-Electrical Optimization of Cd_{1-x}Zn_xTe/Silicon Tandem Solar Cells. *Materials* **2020**, 13, 1860, <https://doi.org/10.3390/ma13081860>.
16. Husein, I.; Rahmawaty, V.; Kinarya, E.; Patonah, N. The effect of photoconductive mole fraction based on thin film Ba_xSr_{1-x}TiO₃ (X = 0.000; 0.125; 0.250; 0.375; 0.500) on electrical properties and diffusivity coefficient. *Biointerface Research in Applied Chemistry* **2021**, 11, 14956-14963, <https://doi.org/10.33263/BRIAC116.1495614963>.
17. Shockley, W.; Queisser, H.J. Detailed Balance Limit of Efficiency of pn Junction Solar Cells. *J. Appl. Phy.* **1961**, 32, <https://doi.org/10.1063/1.1736034>.
18. Peter, L.M. Towards sustainable photovoltaics: the search for new materials. *Philosophical Transactions of the Royal Society A: Mathematical, Physical and Engineering Sciences* **2011**, 369, 1840-1856, <https://doi.org/10.1098/rsta.2010.0348>.
19. Sordo, S.; Abbene, L.; Caroli, E.; Mancini, A.; Zappettini, A.; Ubertini, P. Progress in the Development of CdTe and CdZnTe Semiconductor Radiation Detectors for Astrophysical and Medical Applications. *Sensors* **2009**, 9, 3491-3526, <https://doi.org/10.3390/s90503491>.
20. Naimov, U.R.; Khamrokulov, R.B.; Sultonov, N.; Akobirova, A.T. Examination of the Structure of CdTe Films Obtained by Vacuum Spraying in a Quasiclosed Volume. *Transactions TSTU* **2019**, 25, 500-507.

21. Sultonov, N.S.; Akobirova, A.T.; Khamrokulov, R.B. Structural changes in single crystals of cadmium telluride upon irradiation with argon ions. *Bulletin of the Tajik National University* **2006**, *2*, 55-58.
22. Touskova, J.; Tosek, J.; Klier, E.; Kužel, R. Preparation and Basic Electrical Properties of CdTe Thin Films. *Phys. Status Solidi* **1979**, *56*, 315-322, <https://doi.org/10.1002/pssa.2210560134>.
23. Sultonov, N.S.; Akobirova, A.T.; Azizov, K.; Khamrokulov, R.B. The structure and electrical properties of CdTe films. *Bulletin of the Tajik National University* **2011**, *6*, 26-31.
24. Makhsudov, B.I.; Akobirova, A. T.; Brinkevich, D. I.; Vabishchevich, N.V.; Golovchuk, G.I.; Lukashevich, M.G. Strength properties of neutrino-irradiated epitaxial CdTe films. *Belarusian state University. Physics* **2018**, *1*, 73-79.
25. Khusainov, A.K.; Sultanov, N.S.; Akobirova, A.T.; Azizov, K.D. Polycrystalline films of cadmium telluride for detecting equipment and solar cells. *International Conference "Physics of condensed 'systems' Proceedings, serial Materials Science* **2001**, *47*.
26. Materials Project: <https://materialsproject.org>.
27. Kohn, W.; Sham, L. Self-Consistent Equations Including Exchange and Correlation Effects. *Physical Review A* **1965**, *140*, 1133-1965, <https://doi.org/10.1103/PhysRev.140.A1133>.
28. Hohenberg, P.; Kohn, W. Inhomogeneous electron gas. *Physical Review B* **1964**, *136*, 864-871, <https://doi.org/10.1103/PhysRev.136.B864>.
29. Koller, D.; Tran, F.; Blaha, P. Merits and limits of the modified Becke-Johnson exchange potential. *Physical Review B* **2011**, *83*, <https://doi.org/10.1103/PhysRevB.83.195134>.
30. Hideaki, T.; Kishi, R.; Nakano, M. The Exchange-Energy Density Functional Based on the Modified Becke-Roussel Model. *J. Chem. Theory Comput.* **2010**, *6*, 647-661, <https://doi.org/10.1021/ct900416x>.
31. Lu, Y.H.; Xu, B.; Zhang, A.H.; Yang, M.; Feng, Y.P. Hexagonal TiO₂ for Photoelectrochemical Applications. *The Journal of Physical Chemistry C* **2011**, *115*, 18042-18045, <https://doi.org/10.1021/jp205439x>.
32. Nematov, D.D.; Khusenzoda, M.A.; Burkhonzoda, A.S.; Kholmurodov, K.T.; Lyubchik, A.; Medhat, I. Investigation of Structural and Optoelectronic Properties of N-Doped Hexagonal Phases of TiO₂ (TiO_{2-x}N_x) Nanoparticles with DFT Realization: OPTIMIZATION of the Band Gap and Optical Properties for Visible-Light Absorption and Photovoltaic Applications. *Biointerface Research In Applied Chemistry* **2021**, *12*, 3836-3848, <https://doi.org/10.33263/BRIAC123.38363848>.
33. Nematov, D. Computer analysis of electronic and structural properties of CsSnI₃:Cl and CsPbI₃:Cl nanocrystals. *Electronic periodical peer-reviewed scientific journal "SCI-ARTICLE.RU"* **2019**, *76*, 187-196. Нематов, Д.; Компьютерный анализ электронных и структурных свойств нанокристаллов CsSnI₃:Cl и CsPbI₃:Cl. *Электронный периодический рецензируемый научный журнал «SCI-ARTICLE.RU»* **2019**, *76*, 187-196.
34. Doroshkevich, O.; Nabiye, A.; Shylo, A.; Pawlukojć, A.; Doroshkevich, V.S.; Glazunova, V.A.; Zelenyak, T.Y.; Doroshkevich, N.; Rahmonov, K.R.; Khamzin, E.; Dilshod, N.; Burkhonzoda, A.; Khuseinov, M.; Kholmurodov, K.; Majumder, S.; Balasoiu, M.; Madadzada, A.; Bodnarchuk, V.I. Frequency modulation of the Raman spectrum at the interface DNA - ZrO₂ nanoparticles. *Egyptian Journal of Chemistry* **2019**, *62*, 13-15, doi:10.21608/EJCHEM.2019.12898.1806.
35. Nematov, D.; Burkhonzoda, A.; Khuseinov, M.; Kholmurodov, K.; Doroshkevich, A.; Doroshkevich, N.; Zelenyak, T.; Majumder, S. Molecular Dynamics of DNA Damage and Conformational Behavior on a Zirconium-Dioxide Surface. *Journal of Surface Investigation: X-ray, Synchrotron and Neutron Techniques* **2019**, *13*, 1165-1184, <https://doi.org/10.1134/S1027451019060430>.
36. Nematov, D.; Burkhonzoda, A.; Khuseinov, M.; Kholmurodov, K.; Doroshkevich, A.; Doroshkevich, N.; Zelenyak, T.; Majumder, S.; Ahmed, R.; Medhat, I. Molecular Dynamics Simulations of the DNA Radiation Damage and Conformation Behavior on a Zirconium Dioxide Surface.. *Egyptian Journal of Chemistry* **2019**, *62*, 149-161.
37. Burkhonzoda, A.; Giyosov, S.; Nematov, D.; Khuseinov, M.; Kholmurodov, H. Quanto-mechanical calculation of the electronic structure of ZrO₂:Ti⁴⁺ in the framework of the density functional theory. *Polytechnic Bulletin. Series: Intellect. Innovation. Investments* **2019**, *3*, 11-17. Бурхонзода, А.; Гиёсов, С.; Нематов, Д.; Хусенов, М.; Холмуродов, Х. Кванто-механический расчет электронного строения ZrO₂:Ti⁴⁺ в рамках теории функционала плотности. *Политехнический вестник. Серия: Интеллект. Инновации. Инвестиции* **2019**, *3*, 11-17.
38. Nematov, D.; Burkhonzoda, A.; Khuseinov, M.; Kholmurodov, K.; Yamamoto, T. First principles analysis of geometrical structure, electronic and optical properties of CsSnI_{3-x}Br_x perovskite for photoelectric applications. *Journal of Surface Investigation: X-ray, Synchrotron and Neutron Techniques* **2021**, *15*, 532-536, <https://doi.org/10.1134/S1027451021030149>.
39. Burkhonzoda, A.S.; Nematov, D.D.; Khodzhakhonov, I.T.; Boboshirov, D.I. Optical properties of nanocrystals of the TiO_{2-x}N_x system. *SCI-ARTICLE.RU* **2021**, *92*, 176-187. Бурхонзода, А.С.; Нематов, Д.Д.; Ходжахонов, И.Т.; Бобошеров, Д.И. Оптические свойства нанокристаллов системы TiO_{2-x}N_x. *Электронный периодический рецензируемый научный журнал «SCI-ARTICLE.RU», серия ОПТИКА* **2021**, *92*, 176-187.
40. Burkhonzoda, A.S.; Nematov, D.D.; Kholmurodov, Kh.T. Structural and electronic properties of nanoscale thin films based on ZrO₂. *SCI-ARTICLE.RU* **2021**, *92*, 143-1152. Бурхонзода, А.С.; Нематов, Д.Д.;

- Холмуродов, Х.Т. Структурные и электронные свойства наноразмерных тонких пленок на основе ZrO_2 . *Электронный периодический рецензируемый научный журнал «SCI-ARTICLE.RU», серия НАНОТЕХНОЛОГИИ*, **2021**, 92, 143-1152.
41. Nematov, D.D. Modeling the impact of ionizing radiation on the process of immobilization of biological molecules. *SCI-ARTICLE.RU* **2020**, 81, 12-35. Нематов, Д.Д. Моделирование воздействия ионизирующего излучения на процесс иммобилизации биологических молекул. *Электронный периодический рецензируемый научный журнал «SCI-ARTICLE.RU», серия нанотехнология* **2020**, 81, ст. 12-35.
42. Nematov, D.D. MD modeling of the processes of interaction and encapsulation of nucleotides in the matrix of a carbon nanotube with gold nanoparticles. *SCI-ARTICLE.RU* **2020**, 83, 71-91. Нематов, Д.Д. МД моделирование процессов взаимодействия и инкапсуляции нуклеотидов в матрице углеродной нанотрубки с наночастицами из золота. *Электронный периодический рецензируемый научный журнал «SCI-ARTICLE.RU», серия: физика, нанотехнология* **2020**, 83, 71-91.
43. Nematov, D.D. Research and optimization of optoelectronic properties of N-doped titanium dioxide ($\text{TiO}_{2-x}\text{N}_x$) nanoparticles for photovoltaic applications. *SCI-ARTICLE.RU* **2021**, 91, 110-130. Нематов, Д.Д. Исследование и оптимизация оптоэлектронных свойств N-легированных наночастиц диоксида титана ($\text{TiO}_{2-x}\text{N}_x$) для фотоэлектрических применений. *Электронный периодический рецензируемый научный журнал «SCI-ARTICLE.RU», серия: физика, нанотехнология* **2021**, 91, 110-130.
44. Monkhorst, J.; Pack, D. Special points for Brillouin-zone integrations. *Physical Review B* **1976**, 13, <https://doi.org/10.1103/PhysRevB.13.5188>.
45. Drew, E.S.; James, R.S.; Sampath, W.S. Co-sublimation of $\text{CdSe}_x\text{Te}_{1-x}$ layers for CdTe solar cells. *Solar Energy Materials and Solar Cells* **2017**, 159, <https://doi.org/10.1016/j.solmat.2016.09.025>.
46. Madelung, O. *Numerical Data and Functional Relationships in Science and Technology. Landolt-Bornstein, New series Group III* **1982**, 1717.
47. Bahloul, B.; Deghfel, B.; Amirouche, L.; Bentabet, A.; Bouhadda, Y.; Bounab, S.; Fenineche, N. Ab initio study of the structural, electronic and optical properties of ZnTe compound. *AIP Conference Proceedings* **2015**, 1653, <https://doi.org/10.1063/1.4914210>.
48. Kane, E. Band Structure of Indium Antimonide. *Journal of Physics and Chemistry of Solids* **1957**, 1, 249-261, [https://doi.org/10.1016/0022-3697\(57\)90013-6](https://doi.org/10.1016/0022-3697(57)90013-6).
49. Adachi, S. Zinc Telluride (ZnTe). In: *Optical Constants of Crystalline and Amorphous Semiconductors*. Adachi, S. Ed.; Springer US: Boston **1999**; pp. 473-486, https://doi.org/10.1007/978-1-4615-5247-5_36.
50. Najm, A.S.; Moria, H.; Ludin, N.A. Areca catechu as photovoltaic sensitizer for dye-sensitized solar cell (DSSC). *Biointerface Research in Applied Chemistry* **2020**, 10, 5636-5639, <https://doi.org/10.33263/briac103.636639>.
51. Zafar, M.; Kashif Masood, M.; Rizwan, M.; Zia, A.; Ahmad, S.; Akram, A.; Bao, C.C.; Shakil, M. Theoretical study of structural, electronic, optical and elastic properties of $\text{Al}_x\text{Ga}_{1-x}\text{P}$. *Optik* **2019**, 182, 1176-1185, <https://doi.org/10.1016/J.IJLEO.2018.12.165>.
52. Landsberg, G.S. Optics: Proc. allowance for universities. M.: Fizmatlit 2003, 498–523.
53. Romeo, A.; Artagiani, E. CdTe-Based Thin Film Solar Cells: Past, Present and Future. *Energies* **2021**, 14, 1684, <https://doi.org/10.3390/en14061684>.
54. Yu, B.; Xu, C.; Xie, M.; Cao, M.; Zhang, J.; Jiang, Y.; Wang, L. Deposition of CdZnTe Films with CSS Method on Different Substrates for Nuclear Radiation Detector Applications. *Crystals* **2021**, 12, 187, <https://doi.org/10.3390/cryst12020187>.
55. Tripathy, A.; Behera, M.; Rout, A.S.; Biswal, S.K.; Phule, A.D. Optical, Structural, and Antimicrobial Study of Gold nanoparticles Synthesized Using an Aqueous Extract of Mimosa elengi Raw Fruits. *Biointerface Research in Applied Chemistry* **2020**, 10, 7085-7096, <https://doi.org/10.33263/briac106.70857096>.
56. Tedjini, M.; Oukebdane, A.; Belkaid, M.; Aouail, N. The effect of zinc concentration upon electronic structure, optical and dielectric properties of $\text{Cd}_{1-x}\text{Zn}_x\text{Te}$ alloy: TB-mBJ investigation. *Computational Condensed Matter*. **2021**, 27, 2352-2143, <https://doi.org/10.1016/j.cocom.2021.e00561>.
57. Kheloufi, N.; Bouzid, A. $\text{CdS}_x\text{Te}_{1-x}$ ternary semiconductors band gaps calculation using ground state and GW approximations. *J. Alloys Compd.* **2016**, 671, 144–149, <https://doi.org/10.1016/j.jallcom.2016.02.103>.
58. Levy, M.; Chowdhury, P.; Eller, K.; Chatterjee, A.; Nagpal, P. Tuning ternary $\text{Zn}_{1-x}\text{Cd}_x\text{Te}$ quantum dot composition: engineering electronic states for lightactivated superoxide generation as a therapeutic against multidrug-resistant bacteria. *ACS Biomaterials Science & Engineering* **2019**, 5, 3111–3118, <https://doi.org/10.1021/acsbiomaterials.9b00524>.
59. Rajesh, G.; Muthukumarasamy, N.; Velauthapillai, D.; Mohanta, K.; Ragavendran, V.; Batabyal, S. Photoinduced electrical bistability of sputter deposited CdZnTe thin films. *Materials Research Express* **2018**, 5, <https://doi.org/10.1088/2053-1591/aaad90>.